NASA/TM-2011-217060

Measurement of the Correlation and Coherence Lengths in Boundary Layer Flight Data

Daniel L. Palumbo
Langley Research Center, Hampton, Virginia

February 2011

NASA STI Program . . . in Profile

Since its founding, NASA has been dedicated to the advancement of aeronautics and space science. The NASA scientific and technical information (STI) program plays a key part in helping NASA maintain this important role.

The NASA STI program operates under the auspices of the Agency Chief Information Officer. It collects, organizes, provides for archiving, and disseminates NASA's STI. The NASA STI program provides access to the NASA Aeronautics and Space Database and its public interface, the NASA Technical Report Server, thus providing one of the largest collections of aeronautical and space science STI in the world. Results are published in both non-NASA channels and by NASA in the NASA STI Report Series, which includes the following report types:

- TECHNICAL PUBLICATION. Reports of completed research or a major significant phase of research that present the results of NASA programs and include extensive data or theoretical analysis. Includes compilations of significant scientific and technical data and information deemed to be of continuing reference value. NASA counterpart of peer-reviewed formal professional papers, but having less stringent limitations on manuscript length and extent of graphic presentations.

- TECHNICAL MEMORANDUM. Scientific and technical findings that are preliminary or of specialized interest, e.g., quick release reports, working papers, and bibliographies that contain minimal annotation. Does not contain extensive analysis.

- CONTRACTOR REPORT. Scientific and technical findings by NASA-sponsored contractors and grantees.

- CONFERENCE PUBLICATION. Collected papers from scientific and technical conferences, symposia, seminars, or other meetings sponsored or co-sponsored by NASA.

- SPECIAL PUBLICATION. Scientific, technical, or historical information from NASA programs, projects, and missions, often concerned with subjects having substantial public interest.

- TECHNICAL TRANSLATION. English-language translations of foreign scientific and technical material pertinent to NASA's mission.

Specialized services also include creating custom thesauri, building customized databases, and organizing and publishing research results.

For more information about the NASA STI program, see the following:

- Access the NASA STI program home page at *http://www.sti.nasa.gov*

- E-mail your question via the Internet to help@sti.nasa.gov

- Fax your question to the NASA STI Help Desk at 443-757-5803

- Phone the NASA STI Help Desk at 443-757-5802

- Write to:
  NASA STI Help Desk
  NASA Center for AeroSpace Information
  7115 Standard Drive
  Hanover, MD 21076-1320

NASA/TM-2011-217060

Measurement of the Correlation and Coherence Lengths in Boundary Layer Flight Data

Daniel L. Palumbo
Langley Research Center, Hampton, Virginia

National Aeronautics and
Space Administration

Langley Research Center
Hampton, Virginia 23681-2199

February 2011

Available from:

NASA Center for AeroSpace Information
7115 Standard Drive
Hanover, MD 21076-1320
443-757-5802

I. Abstract

Wall pressure data acquired during flight tests at several flight conditions are analyzed and the correlation and coherence lengths of the data reported. It is shown how the frequency bandwidth of the analysis biases the correlation length and how the convection of the flow acts to reduce the coherence length. Coherence lengths measured in the streamwise direction appear much longer than would be expected based on classical results for flow over a flat plat.

II. Introduction

Correlation length is a measure of the extent of spatially coherent power in the wall pressure and is thus an important parameter in studies of structural response to boundary layer excitation[1,2,3]. It has been established, based on data acquired over several years[4], that the coherent power in the wall pressure decays exponentially with distance. This behavior is reflected in most models of the wall pressure cross spectrum[5,6,7]. The models also assume that the wall pressure statistics are homogeneous and stationary[5,8], that is, the wall pressure can be considered a single process and statistical quantities such as the power spectrum and cross spectrum are constant over the space/time dimensions of the analyses. Assuming stationarity, the cross spectrum can be derived by scaling the power spectrum according to a coherence length* and adjusting the phase according to the convection wavenumber. This is the basis of the Corcos model[5]. As explained in later sections, the coherence length is similar, but not equivalent, to the correlation length. In the Corcos model, the coherence length is inversely proportional to frequency leading to the unrealistic (in light of available data) prediction that the coherence length in the wall pressure would tend towards infinity as the frequency approached zero. This shortcoming in the Corcos model was addressed by Efimtsov[6] who used boundary layer thickness, δ, friction velocity, u_τ, and Strouhal number, S_h, to fit the coherence length to available data. Several other models have since been proposed (see Graham[9] and Hwang[10] for overviews). The purpose of this study is not to select the best model, but to establish a better understanding of the underlying behavior that these models attempt to capture. The Corcos/Efimtsov model will be used to relate the current data and analyses to established norms. The data that forms the basis for the study were acquired in a flight test that was a cooperative venture between the Gulfstream Aerospace Corporation, Boeing Commercial Airplanes and the National Aeronautics and Space Administration (NASA). Previous flight data had issues relating to the installation of sensors flush to the surface of the fuselage despite best efforts to achieve a smooth surface[11,12]. The subject data set was acquired using a pinhole array machined in a single piece of stainless steel sheet metal yielding a surface with minimal irregularities. As will be shown, the data are remarkably consistent over the array. The high quality of the data raises confidence in results that show coherence lengths in the streamwise direction several times longer than expected based on previous studies. Values often quoted in the literature for the Efimtsov model's three parameters for streamwise coherence length (a_1, a_2, a_3) are 0.1, 75.4 and 1.54[6] and predict a coherence length of 0.1 m at 1 kHz. Analysis of the data reveal a coherence length of 0.45 m at 1 kHz requiring parameters of 0.06, 15 and 3. Another recent study also reports a similar trend towards increased measured coherence lengths requiring modifications to model parameters[13]. The observed increased coherence lengths may be due to improved instrumentation[12] as well as the conditions under which the data were acquired as will be discussed in the text. It will be shown that the value of a derived power decay parameter depends on the analysis, i.e., whether it is cross correlation or cross spectrum, and that these analyses can return different results depending on the bandwidth and bin width employed.

The components of the flight test instrumentation and flight test conditions will be described in the next section. The quality of the data will then be evaluated followed by a discussion on the difference between the streamwise and cross stream results. The theoretical basis for computing the correlation and coherence lengths is established followed by a demonstration of the biased behavior of the cross correlation and cross spectrum when operating on turbulent boundary layer wall pressure data.

III. The Flight Test

The flight test was conducted as a cooperative effort between the Gulfstream Aerospace Corporation, Boeing Commercial Airplanes and NASA. The Gulfstream aircraft (a G550) was chosen primarily because its large windows provide a good platform for a long, streamwise, array of sensors that could be built into a window blank.

---

* The term 'coherence length' is introduced here to remove ambiguities on how the quantity is calculated and used.

(a)

(b)

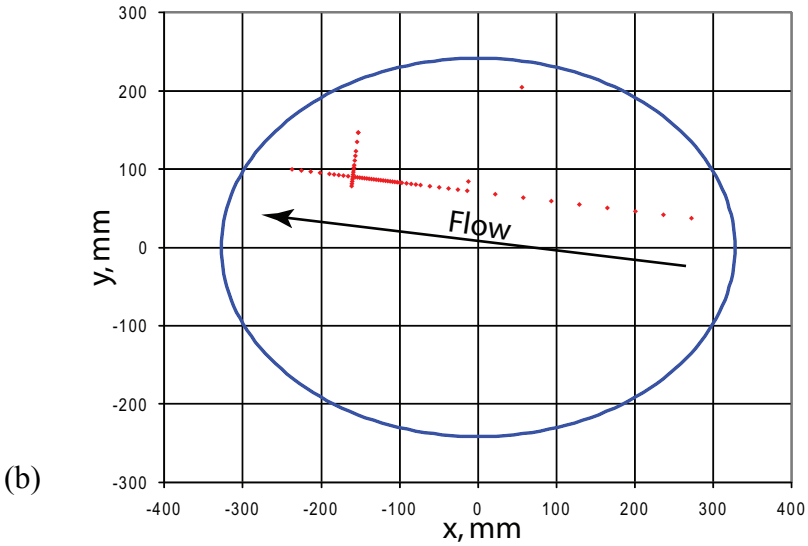

Fig. 1 Flight test vehicle, (a) and position of array in window blank, (b).

A. The test bed and instrumentation

The sensor array was located in the first window of the G550, 6.7 m from the nose of the aircraft on the starboard side, Fig. 1(a). The array was inclined at an angle of 5.5° to the fuselage axis to account for the angle of attack and flow over the body during cruise, Fig. 1(b). The window immediately aft of the test window was marked with a line in the same relative position as the streamwise array and tufts fitted so that the streamline could be observed and the aircraft made to hold the required angle of attack during data acquisition. There were a total of 43 sensors in the streamwise array spanning 47.7 cm and 15 sensors in the cross stream array spanning 8.1 cm. The sensors in the high density portions of the arrays were spaced 3 mm apart. Additional sensors spaced at 6 mm, 12 mm and 36 mm were added to increase the length of the arrays beyond the point of expected significant correlation. The pressure sensors were 1.6 mm in diameter with piezoresistive elements operated in differential mode, vented to the cabin. These type of sensors have a wide temperature range (-55° C to 120° C) and a wide dynamic range with an upper frequency limit of 150 kHz. The sensors were AC coupled. The pinholes were 0.5 mm in diameter and 0.254 mm in depth. The cavity above the sensors was 1.8 mm in depth and 1.45 mm in diameter. The usable bandwidth of the array is limited by the Helmholtz resonance of the cavity and the pinhole dimensions. The Helmholtz resonance frequency for the cavity is approximately 15 kHz. At a nominal convection velocity of 150 m/s the correction factor for a sensor diameter of 0.5 mm is less than 5% at 5 kHz[8]. The data were acquired at 204.8 kHz to maximize time resolution and

for 60 seconds to provide adequate time for averaging. The frequency band of primary interest in this study is limited to 3 kHz to avoid the need for correction while still capturing the important behavior. Unless otherwise noted, 250 averages were performed in computing the spectra.

B. Flight test conditions

Data were acquired over a wide range of test conditions in which Mach number, angle of attack and altitude were varied. For the purposes of studying coherence lengths, only those datasets taken under cruise conditions are useful. Those 3 flight conditions are summarized in Table 1 where c is the speed of sound, U_∞ is the free stream velocity, x is the distance from the nose to the window blank, ν is the kinematic viscosity, Re is the Reynolds number based on x, C_f is the coefficient of skin friction, u_τ is the friction velocity and δ is the boundary layer thickness. The aircraft was held at constant Mach number and angle of attack during data acquisition. The following relationships were used to derive the quantities shown in Table 1 given the altitude and Mach number taken from the aircraft's air data computer and the distance from the nose to the window blank. The speed of sound in air, c, and the kinematic viscosity, ν, are taken from the Aerospaceweb's Atmospheric Properties Calculator* which is based on U.S. Standard Atmosphere 1976.

$$U_\infty = M \times c \tag{1}$$

$$Re = xU_\infty / \nu \tag{2}$$

$$\delta = 0.382 x Re^{-0.2} \tag{3}$$

$$C_f = 0.0594 Re^{-0.2} \tag{4}$$

$$u_\tau = \left(0.5 U_\infty^2 C_f\right)^{0.5} \tag{5}$$

Table 1: Flight test conditions and flow parameters

Flight Number	Mach Number	Altitude (ft)	c (m/s)	U_∞ (m/s)	x (m)	ν (m^2/s)	Re	C_f	u_τ (m/s)	δ (m)
B101	**0.86**	**48000**	**295**	**252**	**6.7**	**6.9E-5**	**2.5E7**	**2.0E-3**	**7.9**	**8.5E-2**
B106	**0.7**	**32000**	**301**	**210**	**6.7**	**3.4E-5**	**4.1E7**	**1.8E-3**	**6.3**	**7.7E-2**
B109	**0.57**	**24000**	**311**	**174**	**6.7**	**2.7E-5**	**4.3E7**	**1.8E-3**	**5.2**	**7.6E-2**

IV. The Data

Before evaluating the data, it is instructive to review characterizations of wall pressure spectra that have formed over the years. These are summarized by Hwang[10] based on observations by Blake[14], Farabee[15] and Bull[4] among others. The expected shape of the wall pressure power spectrum is based on a determination of which scaling variables work best in a particular frequency range. Of note is the division of the spectrum into 4 sections, Fig. 2.

* http://www.aerospaceweb.org/design/scripts/atmosphere

The low frequency (up to $\omega\delta/u_t=5$) and mid-frequency ($\omega\delta/u_t<100$) sections are dominated by structure in the outer layer. The high frequencies ($\omega\nu/u_t^2>0.3$) are dominated by structure in the inner layer. The center section exhibits behavior characteristic of the inner and outer layers. It is instructive to note that the wall pressure spectrum in the low and mid frequency ranges are composed of pressure fluctuations impressed on the wall by a physical process that occurs largely in the outer layer, away from the wall while the higher spectral frequencies reflect physical behavior occurring close to wall. This duality contributes to the non-homogeneous nature of the wall pressure. Using the flow parameters in Table 1 and frequency in Hertz, (Hz), the power spectrum level is expected to increase with a slope proportional to f^2 in the low frequency region, up to 65 Hz. The spectrum is then expected to continue to increase in the mid frequencies until it reaches a peak at about 650 Hz. The slope than gradually decreases until it enters the center frequency range at 1.3 kHz where the slope becomes proportional to approximately f^{-1}. The inner scale region is reached at 55 kHz above which the slope becomes proportional to f^{-5}. A well behaved data set should exhibit these characteristic behaviors. The power spectrum for the sensor at the intersection of the streamwise and cross stream arrays for the 0.7M case is shown in Fig. 2 across the full bandwidth. The frequencies mentioned above are marked and the expected slopes indicated as red dashed lines. The spectrum exhibits the expected behavior except for the low frequency region (below 65 Hz) where the spectrum does not roll off with a slope proportional to f^2. The spectrum below the peak (at about 1 kHz) appears to decay with a slope closely proportional to $f^{0.3}$. This is in reasonable agreement with the $f^{0.2}$ slope observed by Leclercq in this region[16]. An anticipated defect occurs above 10 kHz where the effect of the Helmholtz cavity resonance perturbs the spectrum. The true behavior of the spectrum in this region cannot be known, but the shape of the spectrum outside the influence of the cavity resonance appears to be as expected.

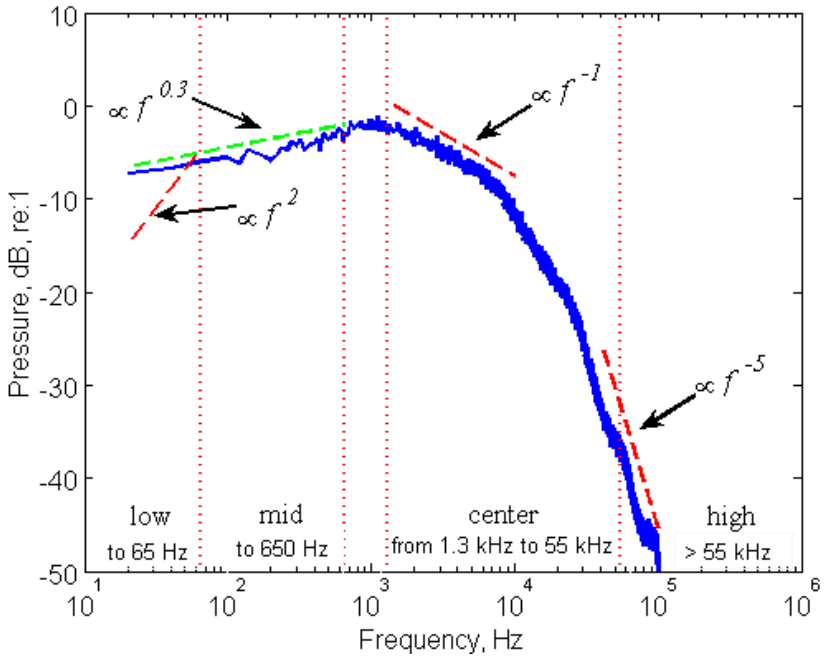

Fig. 2 Power spectrum of a typical sensor at 0.7 M; ---, expected slope; ---estimated slope.

A. Data Consistency

A subset of sensors in both the streamwise and cross stream arrays were sampled and the power spectra and cross spectra compared at each frequency. The cross spectra were taken for pairs of sensors spaced at 3.6 cm for the streamwise array and 0.9 cm for the cross stream array. The distributions of the difference in the power spectra between the sensors in the streamwise array over a band from 100 Hz to 3 kHz are shown in Fig. 3 for the 0.7 M case.

This result is representative of the other 2 flight conditions. For all cases sampled in the streamwise array, 90% of the differences between the power spectra were less than +/- 1 dB and 95% of the differences between the cross spectra were less than +/- 1 dB.

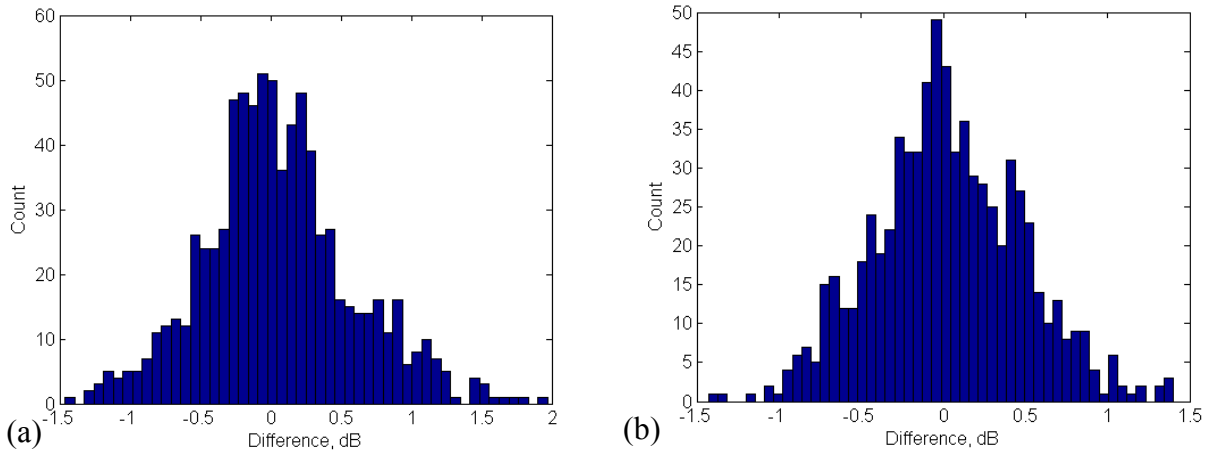

Fig. 3 Differences in power spectrum (a) and cross spectrum at 3.6 cm (b) for sensors in streamwise array at 0.7 M.

The same analysis (except for the cross spectrum being taken at 0.9 cm) for the cross stream array produced less consistent results, Fig. 4. The 0.7 M and 0.56 M cases exhibited similar behavior with 45% of the power spectrum differences below 1 dB and 35% of the cross spectrum differences below 1 dB. The 0.86 M case had much tighter distributions with 70% of the power spectrum differences below 1 dB, and 65% of the cross spectrum differences below 1 dB.

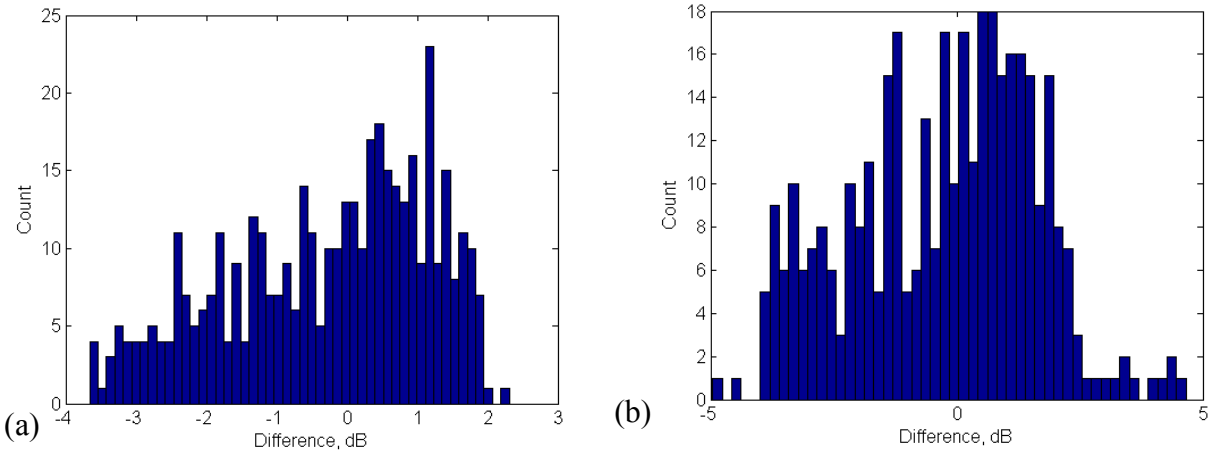

Fig. 4 Differences in power spectrum (a) and cross spectrum at 0.9 cm (b) for sensors in cross stream array at 0.7 M.

The variation in power over the cross stream array is better understood by viewing the individual power spectra. These are shown in Fig. 5 for the 0.7 M case (a) and the 0.86 M case (b). The direction of increasing y dimension is indicated. As can be seen, the levels of both spectra decrease with increasing y. For the 0.7M case (and the 0.56 M case) the overall reduction in level is accompanied by a gradual elimination of the peak at 1 kHz. The power at 1 kHz decreases by nearly 5 dB over the 8.1 cm length of the array at 0.7 M. The spectra at 0.86 M retains its shape, but the

peak is shifted slightly to lower frequencies, decreasing just over 2 dB. The tighter grouping and retention of its basic shape explains why the power differences for the 0.86 M case are less than the 0.7 M and 0.56 M cases. The flattening of the low speed pressure curves with increasing y may indicate a reduction in outer scale influence on the wall pressure that appears to persist at the 0.86M case. The change in pressure over the span of the cross stream array is possibly due to the curvature of the aircraft fuselage. In a study by Heenan[17], data were acquired around the circumference of a cylinder placed at an angle of attack to the flow. This study showed that the pressure spectra on the cylinder exhibited a behavior very similar to that observed here as the sensor locations transitioned from the windward to the leeward side of the cylinder. The difference in behavior between the low speed (0.7 M and 0.56 M) cases and the high speed, 0.855 M, case may be due to a slight difference in angle of attack or the difference in Reynolds number (from Table 1, the Reynolds number for the 0.855 M case is 35% below the lower speed cases).

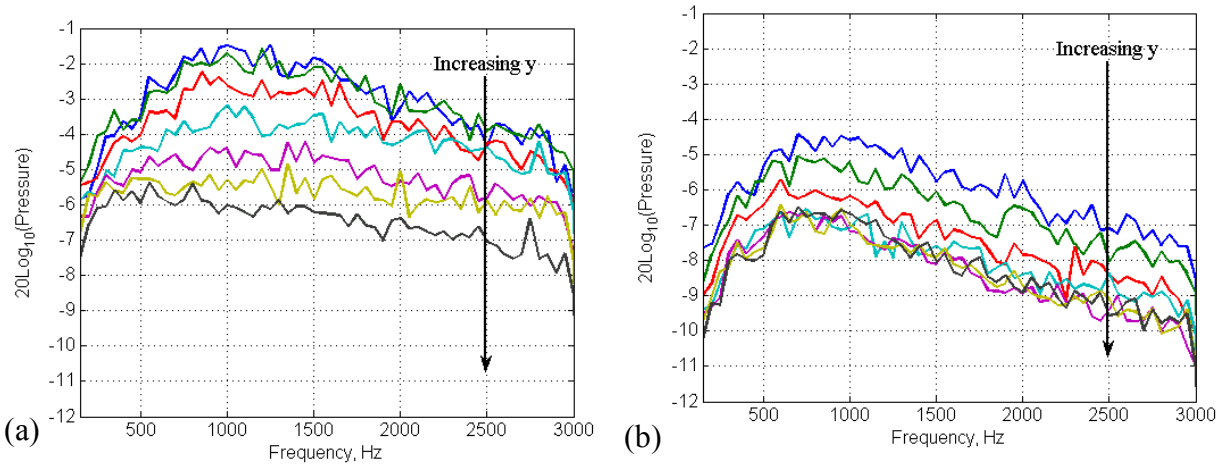

Fig. 5 Power spectra over cross stream array for 0.7 M (a) and 0.86 M (b).

In a previous flight test[18] it was noted that flush mounted sensors, despite best efforts to achieve flushness, could affect sensor phase angle. The phase behavior of the data taken using the pin hole sensors is quite good from very low frequencies up to 10 kHz where the effect of the Helmholtz resonance begins to perturb the phase, Fig. 6.

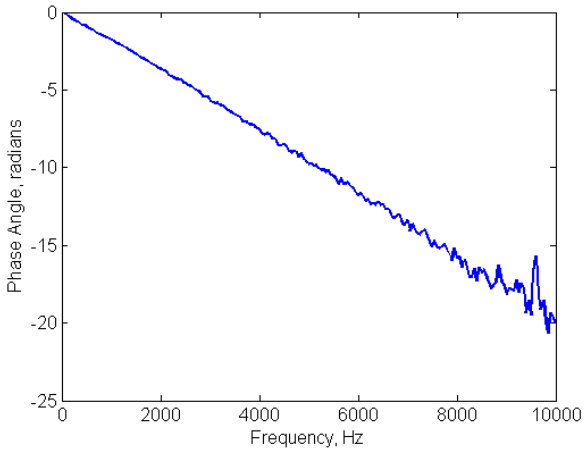

Fig. 6 Cross spectrum phase angle between 2 sensors separated by 2 cm.

B. Confidence Intervals

The primary measurement is that of the instantaneous pressure. The mean of this value is artificially forced to zero as the data were acquired AC coupled. Better measures, and ones more related to the subject matter of this paper, are the mean square power and the mean cross power. One sample of the mean power is taken from 4096 pressure measurements. This length ensemble was chosen because it was the smallest length at which the effects of convection are reduced (as will be explained in the following sections). Using this ensemble length, it is possible to take 3,000 samples of the mean power. The large number of samples guarantees a normal distribution according to the Central Limit Theorem. This is shown to be the case for the mean square power in Fig. 7(a). The mean cross power was similarly distributed. The confidence interval for a normally distributed random variable with unknown standard deviation is[19]

$$ci(\alpha, n, s) = \pm t_{1-\frac{\alpha}{2}, n-1}\left(\frac{s}{\sqrt{n}}\right),$$

where ci is the confidence interval, α is the complement of the desired probability that the measurement is in the interval, t is the Student's t distribution, n is the number of samples and s is the standard deviation of the sample set. Using n=3000, s = 0.618 and α=0.01, the mean square power is 127 dB with a 99% confidence interval of 0.029 dB. The mean cross power is found to be 125 dB with a 99% confidence interval of 0.026 dB. A similar analysis was done in the frequency domain with the results shown in Fig. 7(b). The frequency domain confidence intervals are an order of magnitude greater than the time domain values, but are still only a fraction of a dB.

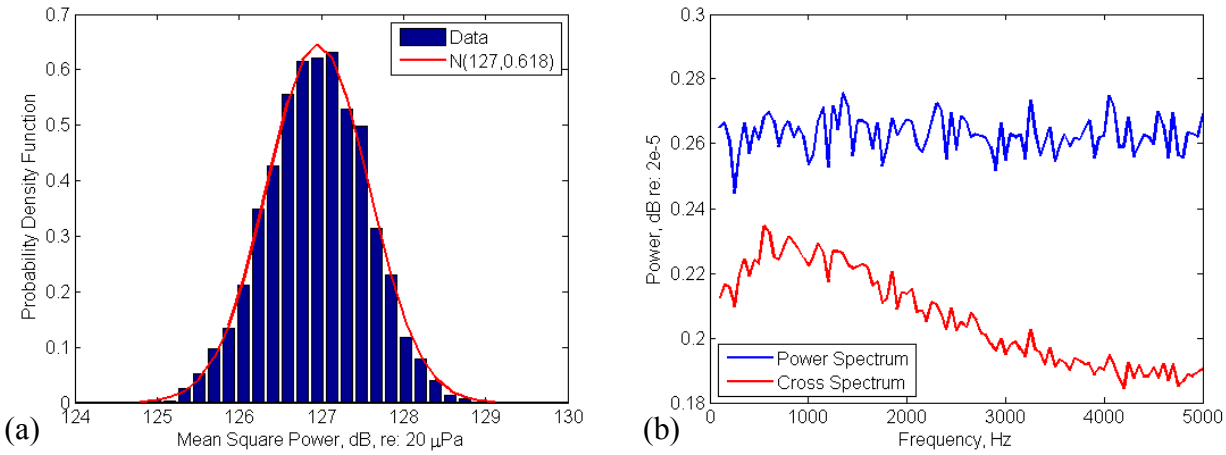

Fig. 7 Distribution of samples of mean square power, (a), confidence intervals in frequency domain, (b).

V. Correlation and Coherence Length Analyses

The term 'correlation length' is often used to describe coherent power decay rates derived by both the cross correlation and the cross spectrum. The resulting rates are quite different, however, and using the same term for both quantities introduces ambiguity. In this study, the term correlation length will be used to describe power decay rates computed using the cross correlation and 'coherence length' for rates computed using the cross spectrum. The space-time cross correlation in one spatial dimension is written as

$$\chi(x_0, x_1, t_0, \tau) = \langle p((x_0, t_0) \cdot p(x_1, t_0 + \tau)) \rangle \tag{6}$$

Here $p(x,t)$ is the pressure at some point in space and time and the brackets, $\langle \ldots \rangle$, denotes the average over N samples in time. The power decay rate is determined from cross correlation analysis by fitting an exponential distribution to the peaks in the cross correlation taken from a reference sensor to other sensors in the array, see Eq. 7 and Fig. 8(a).

$$max(\chi(x_0, x_i, t_0, \tau)) \cong e^{-\frac{|x_0 - x_i|}{L}} \tag{7}$$

The correlation length, L, is determined by the value that produces the best fit over all the correlation peaks. Note that the cross correlation is normalized to the RMS power in each sensor so that the peak in the auto correlation is 1.

The space-time correlation is related to the cross spectrum by the Fourier transform.

$$\phi(x_0, x_1, t_0, f) = \int_N \chi(x_0, x_1, t_0, \tau) e^{-i2\pi f\tau} d\tau \tag{8}$$

For a discrete Fourier transform, the integral is taken over N samples in time and produces one ensemble of cross spectrum. If the data were acquired at a sample rate f_s, the bandwidth of the spectrum would be $f_s/2$ with (N+1)/2 frequency bins of width f_s/N. The cross spectrum magnitudes are normalized by the square root of the respective auto spectra so that the resulting quantity is equivalent to the square root of the coherence.

$$\gamma(x_0, x_1, t_0, f) = \frac{\left|\phi(x_0, x_1, t_0, f)\right|}{\left|\phi(x_0, x_0, t_0, f)\right|^{0.5} \left|\phi(x_1, x_1, t_0, f)\right|^{0.5}} \tag{9}$$

The coherence length for a particular frequency is found by fitting an exponential to γ at that frequency.

$$\gamma(x_0, x_i, t_0, f_j) \cong e^{-\frac{|x_0 - x_i|}{L_j}} \tag{10}$$

An example of an exponential fit to γ in the streamwise direction at 1.5 kHz is shown in Fig. 8(b). Two things are immediately obvious when comparing the coherence length in Fig. 8(b) to the correlation length in Fig. 8(a). First, the coherence length has a much better fit to the exponential than the correlation length. This is true at all frequencies. Second, the coherence length at this frequency is much longer than the correlation length. Both these observations can be understood by considering the plot in Fig. 9 of the coherence length over the band from 100 Hz to 30 kHz.

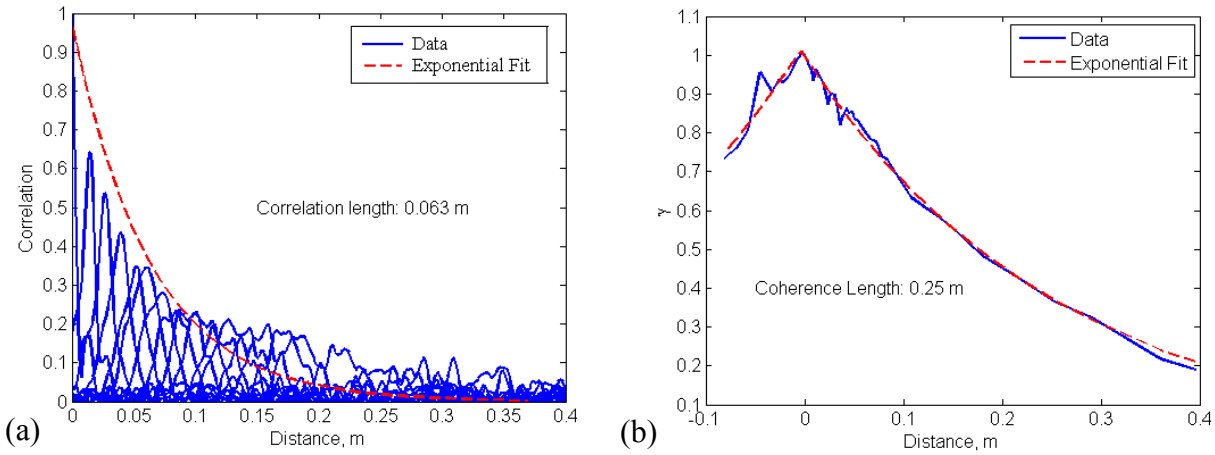

Fig. 8 Correlation length determined by exponential fit to peaks in cross correlation, (a) and coherence length determined by exponential fit to cross spectrum magnitude at 1500 Hz, (b)

The coherence length is strongly frequency dependent reaching its maximum at frequencies corresponding to the peak in the power spectrum, i.e., ~ 1 kHz, and decreasing rapidly at higher frequencies. At high frequencies, structures in the inner layer which decay rapidly dominate the wall pressure behavior. At low frequencies, structures in the outer layer dominate with much longer decay lengths. The cross correlation is a wide band analysis in that its result is a combination of these behaviors over all frequencies. At short distances the short decay lengths of the structures at the higher frequencies causes a rapid fall off in correlated power and at greater distances, the longer decay lengths of the low frequency structures sustain the correlated power. The lack of consistency in the correlation decay processes across the frequency band results in a behavior that cannot be adequately modeled by a single exponential curve. This is the reason for the less than optimal fit in Fig. 8(a) at greater distances.

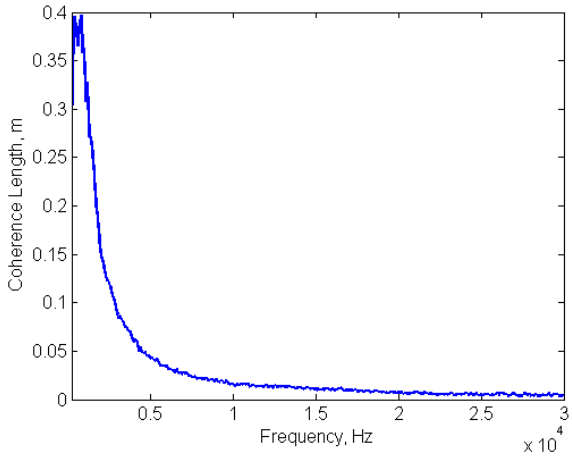

Fig. 9 Coherence length 100 Hz to 30 kHz.

The disparity in behavior can be reduced by narrowing the analysis frequency band to a region of interest, for example, around the 1 kHz peak in the power spectrum. The result of deriving the correlation length from data that was band limited to the frequency range of 100 Hz to 3 kHz is shown in Fig. 10(a). At this analysis bandwidth, the correlation length (0.23m) is far greater then that obtained using the data's full bandwidth, shown in Fig. 8(a), and illustrates the effect of removing most of the high frequency, inner layer, behavior. The correlation length will approach the coherence length as the frequency band is narrowed. The coherence length at this bandwidth is shown

in Fig. 8(b) and is, of course, unchanged. At this point, one might conclude that the cross spectrum is the more reliable statistic. That is not entirely the case as will be demonstrated in the following sections.

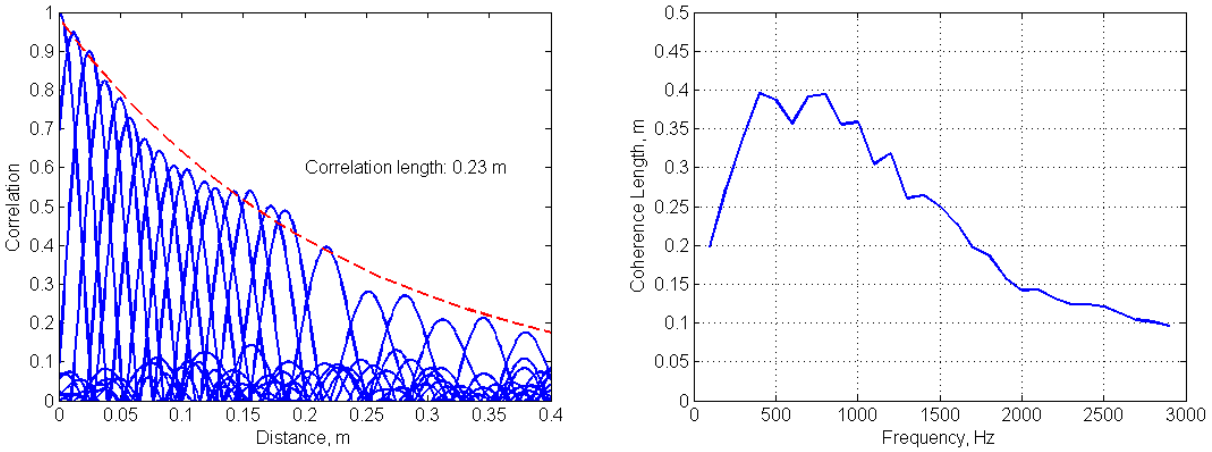

Fig. 10 Correlation length, (a), and coherence length, (b), computed over a frequency band from 100 Hz to 3 kHz.

A. Effects of convection and ensemble length.

The coherence length result shown in Fig. 10(b) was computed with an ensemble length of 2048 samples resulting in a bin width of 100 Hz. Unfortunately, the coherence length computation depends on ensemble length, converging with longer lengths, Fig. 11. Care must be taken to use ensemble lengths long enough to accurately estimate the coherence length. The quality of fit of the exponential to the coherence decay is not altered as the ensemble length is varied and remains very good, e.g. see Fig. 8(b).

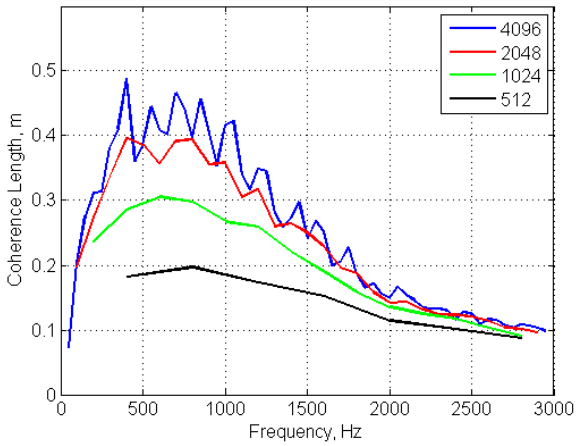

Fig. 11 Coherence length computed at several ensemble lengths.

VI. Data Analysis

A cross spectrum with a 4096 ensemble length and 50 Hz bin was used to analyze the flight data. The coherence length will be compared to historic values by comparison to Corcos and Efimtsov model parameters most often quoted in the literature, for example by Graham[1].

The Corcos model[5] for the cross spectrum assumes an exponential decay of correlated power with distance and can be written as:

$$\phi(r_1, r_2, \omega) = e^{-\alpha_1 \omega |r_1| / U_c} e^{-\alpha_2 \omega |r_2| / U_c} e^{i \omega r_1 / U_c} \tag{11}$$

Here r_1,α_1 and r_2,α_2 are the distance between two points and the decay constant for the streamwise and cross stream directions, respectively. The coherence length, L_{coh}, is then

$$L_{coh,\,C} = \frac{U_c}{\alpha \omega} \tag{12}$$

The predicted coherence length is inversely proportional to frequency leading to over estimation of the value at low frequency when compared to actual data. Efimtsov[6] offered a correction for the coherence length as

$$L_{coh,\,E} = \delta \left[\left(\frac{a_1 Sh}{U_c / u_\tau} \right) + \frac{a_2^2}{Sh^2 + (a_2 / a_3)^2} \right]^{1/2}, \tag{13}$$

where δ is the boundary layer thickness, Sh is the Strouhal number, u_τ is the friction velocity and parameters $a_{1..3}$ are defined specifically for the streamwise and cross stream directions. The values of these parameters most often used in the literature are given in Table 2 along with values derived from the flight test data. The Efimtsov model is constrained by the Corcos model (through a_1) at mid to high frequencies. Parameter a_2 controls where the Efimtsov model breaks away from the Corcos curve. Parameter a_3 controls the low frequency roll off. The frequency and height of the peak in the coherence length curve can then be set by adjusting a_1, a_2 and a_3.

Table 2: Coherence length parameters.

	Streamwise			Cross Stream		
	$a_1=\alpha_1$	a_2	a_3	$a_1=\alpha_2$	a_2	a_3
Graham[1]	**0.1**	**72.8**	**1.54**	**0.77**	**548**	**13.5**
0.57 M	**0.06**	**5.0**	**1.0**	**0.77**	**260**	**4.0**
0.7 M	**0.06**	**5.0**	**1.0**	**0.77**	**260**	**4.0**
0.86 M	**0.07**	**4.0**	**1.0**	**0.85**	**60**	**4.0**

Fig. 12(a) illustrates the fit of the Corcos and Efimtsov models to the 0.7 M streamwise coherence length data. The fit is a compromise in that some error must be tolerated at the high frequencies to raise the curve to match the peak at lower frequencies. The changes in the parameters reflect an observed increase in coherence length. The original Efimtsov parameters predicted a maximum streamwise coherence length of 0.1 m at 1.5 kHz. Analysis of the

flight data has the coherence length peaking at close to 0.5 m at 750 Hz. Note that all flight conditions returned similar values for a_1, a_2 and a_3 indicating a consistent result. The cross stream cases were less well behaved, Fig. 12(b). The Corcos parameter, a_1, was unchanged for the 0.57 M and 0.7 M cases and required a slight increase for the 0.86 M case. The a_2 parameter had to be reduced by 50% for the lower speed cases and nearly 90% for the 0.86 M case. The reduction in a_2 for the 0.86 M cross stream case is of the same order as that required in a_2 for the streamwise case. The reason for this, as described earlier in section "IV.A. Data Consistency", is that the 0.86M cross stream spectrum maintained a pressure response indicative of outer layer coherent structure that diminishes at the slower speeds. The behavior of the wall pressure under these flight conditions appears to be much different than that observed under the controlled laboratory conditions in which the historic models and parameters where derived.

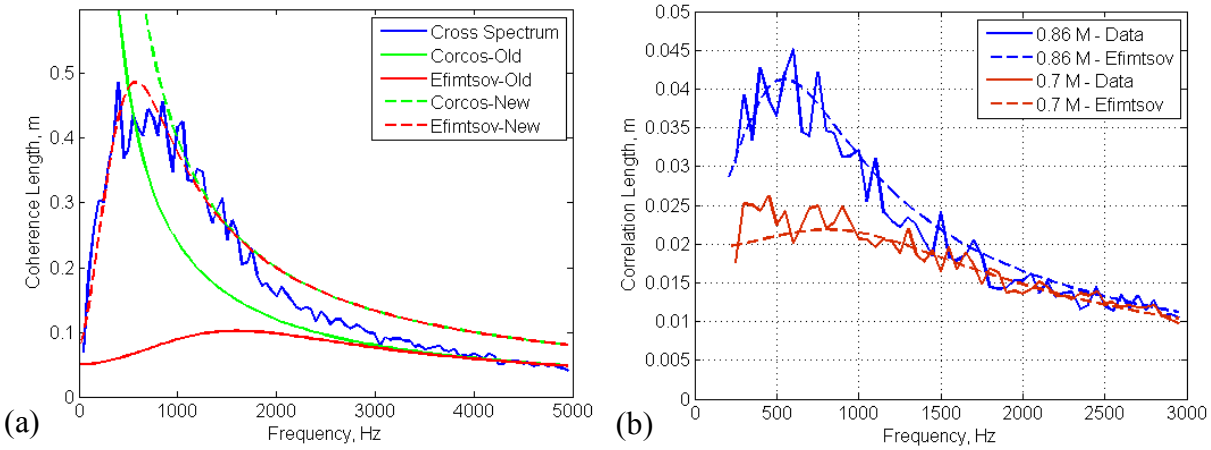

Fig. 12 Coherence length dependence on frequency for 0.7 M streamwise case (a), and, comparison of 0.7 M and 0.86 M cross stream cases, (b)

VII. Conclusions

For the purpose of determining the parameters for models which estimate the wall pressure of the turbulent boundary layer over the surface of an aircraft fuselage, the current data are inadequate. Although it has been argued that the data are of high quality, the variation in pressure levels and spectra shape along the cross stream array leads one to conclude that a single set of parameters extracted from data taken at one location on the fuselage are insufficient. Thus, more tests are necessary to validate the observed behavior including the very long coherence lengths and especially the hypothesis that fuselage curvature modulates the influence of outer layer structure on the wall pressure. Given the available data, the Efimtsov model is able to adequately describe the coherence length frequency dependency although the result is a compromise between best fit for the lower versus the higher frequency ranges. To match observed coherence lengths that were almost five times longer than predicted, it was necessary to make considerable changes to the accepted Efimtsov parameters.

The different turbulent mechanisms that are at work in the inner and outer layers produce a frequency dependence that may bias wide band analyses such as the cross correlation. Error in the cross spectrum due to a shift in the data caused by convection may be reduced by using long ensemble lengths and narrow bin widths.

VIII. References

[1]Graham, W.R., "Boundary layer induced noise in aircraft, Part I: The flat panel model", *Journal of Sound and Vibration*, Vol. 192(1), pp. 101-120, 1996.

[2]Maury, C., Gardonio, P., and Elliott, S. J., "A wavenumber approach to modelling the response of a randomly excited panel, Part II: Application to aircraft panels excited by a turbulent boundary layer", *Journal of Sound and Vibration*, Vol. 252(1), pp. 115-139, 2002.

[3]Hambric, S.A., Hwang, Y.F., and Bonness, W.K., "Vibrations of plates with clamped and free edges excited by low-speed turbulent boundary layer flow", *Journal of Fluids and Structures*, Vol. 19, pp. 93-110, 2004.

[4]Bull, M.K., "Wall-pressure fluctuations beneath turbulent boundary layers: some reflections on forty years of research", *Journal of Sound and Vibration*, Vol. 190(3), pp. 299-315, 1996.

[5]Corcos, G.M., "The structure of the turbulent pressure field in boundary-layer flows", *Journal of Fluid Mechanics*, Vol. 18, pp. 353-378, 1963.

[6]Efimtsov, B.M., "Characteristics of the field of turbulent wall pressure fluctuations at large reynolds numbers", *Sov. Phys. Acoust.*, Vol. 28(4), pp. 289-292, 1982.

[7]Chase, D.M., "The character of the turbulent wall pressure spectrum at subconvective wavenumbers and a suggested comprehensive model", *Journal of Sound and Vibration*, Vol. 112(1), pp. 125-147, 1987.

[8]Corcos, G.M., "Resolution of pressure in turbulence", *Journal of Acoustical Society of America*, Vol. 35(2), pp. 192-199, 1963.

[9]Graham, W.R., "A comparison of models for the wavenumber-frequency spectrum of turbulent boundary layer pressures", *Journal of Sound and Vibration*, Vol. 206(4), pp. 541-565, 1997.

[10]Hwang, Y.F., Bonness, W.K., and Hambric, S.A., "Comparison of semi-empirical models for the turbulent boundary layer wall pressure spectra", *Journal of Sound and Vibration*, Vol. 319, pp. 199-217, 2009.

[11]Rizzi, S.A., Rackl, R.G., & Andrianov, E.V., "Flight test measurement from the TU-144LL structure/cabin noise experiment", NASA TM-2000-209858, 2000.

[12]Efimtsov, B.M, Golubev, A.Y, Kuznetsov, V.B, Rizzi, S.A., Andersson, A.O, Rackl, R.G., and Andrianov, E.V., "Effect of transducer flushness on measured surface pressure fluctuations in flight", AIAA Paper 2005-0800, Jan. 2005.

[13]Finnveden, S., Birgersson, F., Ross, U., and Kremer, T., "A model of wall pressure correlation for prediction of turbulence-induced vibration", *Journal of Fluids and Structures*, Vol. 20, pp. 1127-1143, 2005.

[14]Blake, W.K., *Mechanics of flow-induced sound and vibration, Vols. I and II,* Academic Press, New York, 1986.

[15]Farabee, T.M. and Casarelle, M.J., "Special features of wall pressure fluctuations beneath turbulent boundary layers", *Physics of Fluids A*, Vol. 3(10), pp. 2410-2420, 1991.

[16]Leclercq, D.J., and Bohineust, X., "Investigation and modelling of the wall pressure field beneath a turbulent boundary layer at low and medium frequencies", *Journal of Sound and Vibration*, Vol. 257(3), pp. 477-501, 2002.

[17]Heenan, A.F., and Morrison, J.F., "Turbulent boundary layers on axially inclined cylinders. Parts 1", *Experiments in Fluids*, Vol. 32, pp. 547-557, 2002.

[18]Palumbo, D, "Characteristic lifelength of coherent structure in the turbulent boundary layer", *AIAA Journal*, Vol. 6. No. 4, pp. 810-823, April, 2008.

[19]Canavos, G.c., *Applied Probability and Statistical Methods*, Little, Brown and Co., Boston, 1984.

REPORT DOCUMENTATION PAGE

Form Approved
OMB No. 0704-0188

1. REPORT DATE *(DD-MM-YYYY)*	2. REPORT TYPE	3. DATES COVERED *(From - To)*
01- 02 - 2011	Technical Memorandum	

4. TITLE AND SUBTITLE
Measurement of the Correlation and Coherence Lengths in Boundary Layer Flight Data

5a. CONTRACT NUMBER

5b. GRANT NUMBER

5c. PROGRAM ELEMENT NUMBER

6. AUTHOR(S)
Palumbo, Daniel L.

5d. PROJECT NUMBER

5e. TASK NUMBER

5f. WORK UNIT NUMBER
561581.02.08.07.18.15

7. PERFORMING ORGANIZATION NAME(S) AND ADDRESS(ES)
NASA Langley Research Center
Hampton, VA 23681-2199

8. PERFORMING ORGANIZATION REPORT NUMBER
L-19938

9. SPONSORING/MONITORING AGENCY NAME(S) AND ADDRESS(ES)
National Aeronautics and Space Administration
Washington, DC 20546-0001

10. SPONSOR/MONITOR'S ACRONYM(S)
NASA

11. SPONSOR/MONITOR'S REPORT NUMBER(S)
NASA/TM-2011-217060

12. DISTRIBUTION/AVAILABILITY STATEMENT
Unclassified - Unlimited
Subject Category 01
Availability: NASA CASI (443) 757-5802

13. SUPPLEMENTARY NOTES

14. ABSTRACT

Wall pressure data acquired during flight tests at several flight conditions are analyzed and the correlation and coherence lengths of the data reported. It is shown how the frequency bandwidth of the analysis biases the correlation length and how the convection of the flow acts to reduce the coherence length. Coherence lengths measured in the streamwise direction appear much longer than expected.

15. SUBJECT TERMS
Correlation length; Coherence length; Boundary layer

16. SECURITY CLASSIFICATION OF:			17. LIMITATION OF ABSTRACT	18. NUMBER OF PAGES	19a. NAME OF RESPONSIBLE PERSON
a. REPORT	b. ABSTRACT	c. THIS PAGE			STI Help Desk (email: help@sti.nasa.gov)
					19b. TELEPHONE NUMBER *(Include area code)*
U	U	U	UU	19	(443) 757-5802